Published in final edited form as:

J Am Chem Soc. 2022 November 16; 144(45): 20641–20652. doi:10.1021/jacs.2c07224.

Nonheme Iron(III) Azide and Iron(III) Isothiocyanate Complexes: Radical Rebound Reactivity, Selectivity, and Catalysis

Vishal Yadav[†], **Lyupeng Wen**[†], **Rodolfo J. Rodriguez**[†], **Maxime A. Siegler**[†], **David P. Goldberg**[*,†]

[†] Department of Chemistry, The Johns Hopkins University, 3400 North Charles Street, Baltimore, Maryland, 21218, USA

Abstract

The new nonheme iron complexes $Fe^{II}(BNPA^{Ph2}O)(N_3)$ (**1**), $Fe^{III}(BNPA^{Ph2}O)(OH)(N_3)$ (**2**), $Fe^{II}(BNPA^{Ph2}O)(OH)$ (**3**), $Fe^{III}(BNPA^{Ph2}O)(OH)(NCS)$ (**4**), $Fe^{II}(BNPA^{Ph2}O)(NCS)$ (**5**), $Fe^{III}(BNPA^{Ph2}O)(NCS)_2$ (**6**), and $Fe^{III}(BNPA^{Ph2}O)(N_3)_2$ (**7**) ($BNPA^{Ph2}O$ = 2-(bis((6-(neopentylamino)pyridin-2-yl) methyl)amino)-1,1-diphenylethanolate) were synthesized and characterized by single crystal X-ray diffraction (XRD), as well as by ^1H NMR, ^{57}Fe Mössbauer and ATR-IR spectroscopies. Complex **2** was reacted with a series of carbon radicals, $Ar^X{}_3C\bullet$ (Ar^X = *p*-X-C_6H_4), analogous to the proposed radical rebound step for nonheme iron hydroxylases and halogenases. The results show that for $Ar^X{}_3C\bullet$ (X = Cl, H, ^{t}Bu), only OH• transfer occurs to give $Ar^X{}_3COH$. However, when X = OMe, a mixture of alcohol ($Ar^X{}_3COH$) (30%) and azide ($Ar^X{}_3CN_3$) (40%) products was obtained. These data indicate that the rebound selectivity is influenced by the electron-rich nature of the carbon radicals for the azide complex. Reaction of **2** with $Ph_3C\bullet$ in the presence of Sc^{3+} or H^+ reverses the selectivity, giving only the azide product. In contrast to the mixed selectivity seen for **2**, the reactivity of *cis*-$Fe^{III}(OH)(NCS)$ with the X = OMe radical derivative leads only to hydroxylation. Catalytic azidation was achieved with **1** as catalyst, λ^3-azidoiodane as oxidant and azide source, and Ph_3CH as test substrate, giving Ph_3CN_3 in 84% (TON = 8). These studies show that hydroxylation is favored over azidation for nonheme iron(III) complexes, but the nature of the carbon radical can alter this selectivity. If an OH• transfer pathway can be avoided, the $Fe^{III}(N_3)$ complexes are capable of mediating both stoichiometric and catalytic azidation.

Graphical Abstract

[*]**Corresponding Author** dpg@jhu.edu.

ASSOCIATED CONTENT

Supporting Information

This material is available free of charge via the internet at http://pubs.acs.org

X-ray crystallographic data for **1** – **7** (CIF)

Syntheses, ^1H NMR spectra, ^{57}Fe Mössbauer data, UV-vis spectra, IR spectra, supporting tables S1–S8 and supporting Figures S1–S56 (PDF).

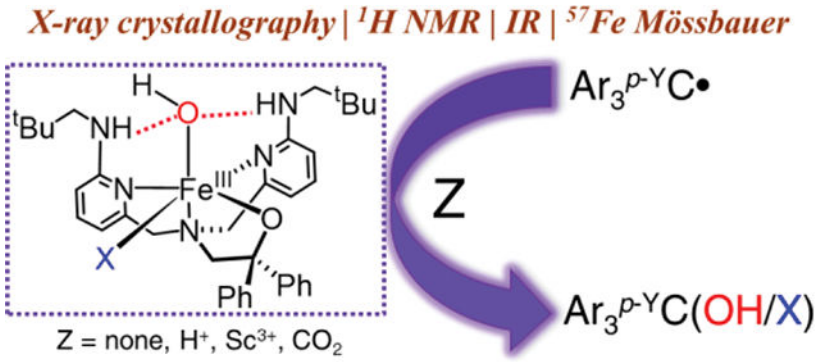

X	Y	product(s)
N_3	Cl	*hydroxylation only*
	OMe	*hydroxylation + azidation*
NCS	OMe	*hydroxylation only*
	Cl	*no reaction*

Introduction.

Nature employs a variety of heme and nonheme iron enzymes to carry out the oxidation of C-H substrates with dioxygen as the biological oxidant.[1–4] These oxidations include a broad range of transformations, including C-H hydroxylation and C-H halogenation. Efforts in protein engineering have led to these abiological transformations being catalyzed by appropriately modified metalloenzymes.[5] A reaction of particular synthetic significance is azidation, wherein a selective R-H bond is converted into an R-N_3 group. The resulting organoazide is a useful synthon for constructing a variety of different organic compounds with pharmaceutical and other industrial applications.[6–9] Organoazides can be considered as pseudohalogens, and a straightforward approach toward developing an azidation catalyst involves converting a halogenase into an azidase,[10–12] with the addition of an exogenous azide source (Scheme 1). The nonheme iron enzyme SyrB2 (involved in biosynthesis of syringomycin E) normally carries out halogenation of its native substrate L-threonine, but its reactivity can be extended to give an azidation product in the presence of NaN_3 as the azide source.[10] The HalB (a lysine halogenase) enzyme carries out halogenation of freestanding amino acids, and exhibits moderate yields of azidation products in the presence of an external azide source.[11] A relatively new class of plant halogenase, dechloroacutumine halogenase (DAH), mediates a terminal C-H halogenation step in the biosynthesis of tetracyclic chloroalkaloid (−)-acutumine. This enzyme is capable of azidation, but attempts to install other functional groups such as Br, NCS, NCO, NO_2 were unsuccessful.[12]

In related efforts, attempts to convert the nonheme iron 2-(oxo)-glutarate (2OG)-dependent hydroxylases into halogenases initially involved the seemingly straightforward deletion of the conserved Asp/Glu ligand in the His-X-(Asp/Glu)-Xn-His metal-binding motif. It is

this conserved carboxylate ligand that is absent in the analogous Fe^{II}/2-OG-dependent halogenases, being replaced by a halogen atom for transfer to substrate. However, this straightforward strategy of carboxylate ligand deletion failed to lead to halogenation reactivity, until a structure-guided bioinformatics approach was taken which led to the discovery of the hydroxylase SadA. A single site variant of SadA (D157G) does show some halogenase activity, albeit at low levels.[13] Reprogramming of another hydroxylase into a halogenase was subsequently reported.[14] Other nonnative anions, including N_3^-, were recently tested with an engineered SadA variant ("SadX"), and azidation activity was observed.[15] A non-ferryl mediated C-H azidation reaction with an engineered nonheme Fe dioxygenase was also recently described, relying on a new radical-relay strategy for nonnative nonheme iron catalysis.[16]

Despite these recent successes, major challenges remain in the general engineering of nonheme iron enzymes to carry out nonnative transformations such as azidation, including the low yields and poor stereoselectivity typically observed in these reactions. It is reasonable to assume that the azidation seen for the halogenases proceeds via a mechanism similar to halogenation,[17] in which a ferryl (*cis*-$Fe^{IV}(O)(N_3)$) species abstracts an H atom from R-H to form a ferric hydroxide (*cis*-$Fe^{III}(OH)(N_3)$) intermediate and a carbon radical (R•). The ferric intermediate, which is depicted in Scheme 1, must then selectively transfer N_3• over OH• to R• to give an azidation (R-N_3) product in a so-called rebound process. Assuming this mechanism is correct, the selectivity, efficiency, and overall yield of azidation critically depends on the factors that control the preferential rebound of N_3• over OH• from the ferric hydroxide intermediate.

A few examples of synthetic transition metal complexes that can serve as catalysts for R-H azidation have been reported.[18–23] A small subset involve nonheme iron complexes,[20–22] and mechanistic analysis has implicated an $Fe^{III}(N_3)$ catalytic intermediate that transfers N_3• to a carbon radical (R•) substrate in a process analogous to the ferric hydroxide-mediated enzymatic reactions. However, the reactivity of isolated, structurally characterized nonheme $Fe^{III}(N_3)$ complexes with carbon radicals has not yet been examined.

We have recently reported the synthesis of isolable, structurally characterized nonheme iron complexes that model the proposed *cis*-$Fe^{III}(OH)(X)$ (X = OTf, halide, OAr, SAr) ferric intermediates in certain nonheme iron enzymes, and examined their competitive radical transfer reactivity with exogenous carbon radicals.[24–27 28–30] These studies showed that the selectivity of OH• versus X• transfer is influenced by bond strengths, the identity of X•, reaction temperature, and the nature of the carbon radical (e.g. 3° versus 2° carbon).

Herein we report the first structurally characterized *cis*-$Fe^{III}(OH)(X)$ (X = N_3, NCS) complexes, prepared with the tetradentate, monoanionic ligand $BNPA^{Ph2}O^-$, which was used in our previous studies and which contains secondary coordination sphere hydrogen bonding groups to help stabilize the terminal hydroxide ligand. These ferric complexes were examined for their reactivity toward triphenylmethyl radical derivatives ((p-X-$C_6H_4)_3C$• where X = OMe, H, ^{t}Bu, Cl),[23, 31–38] providing us with a direct assessment of the ability of these and related ferric complexes to transfer the triatomic pseudohalogen donors N_3^- and NCS^-. These complexes also allowed us to address the influence of exogeneous Lewis (e.g.

Sc^{3+}) or Bronsted acids, as well as CO_2, on the radical rebound selectivity. We also provide proof of concept that catalytic azidation is viable for these nonheme iron complexes.

RESULTS AND DISCUSSION

Synthesis and characterization of iron(II) and iron(III) complexes.

A detailed synthetic route for complexes **1 – 7** is shown in Scheme 2. The iron(II) complex $Fe^{II}(BNPA^{Ph2}O)(N_3)$ (**1**) was synthesized by addition of NaN_3 to the previously reported[29] $Fe^{II}(BNPA^{Ph2}O)(Br)$ complex. Following workup and crystallization from THF/pentane, the product was isolated in moderate to high yield as dark yellow blocks, and structurally characterized by single crystal X-ray diffraction (XRD). The structure revealed the expected five-coordinate iron(II) complex (Figure 1a) with the azide in the hydrogen bonding site and a distorted trigonal bipyramidal (tbp) geometry (τ_5 = 0.69).[39] Treatment of **1** with excess, dry O_2 gas caused an immediate color change from yellow to orange in either THF or CH_3CN. Crystallization from THF/pentane gave bright orange crystals which were identified by XRD as the new iron(III) complex $Fe^{III}(BNPA^{Ph2}O)(OH)(N_3)$ (**2**) (Figure 1b). The structure shows complex **2** is six-coordinate with the azide in a position cis to a terminal OH ligand, which occupies the H-bonding site: N1(H)…O2 = 2.707(3) Å, N5(H)–O2 = 2.748 (2)Å. The Fe–N_3 distance refines to 2.077(2) Å in **2**, and is nearly the same as that seen for **1**.

Complex **1** in THF shows a strong band at 330 nm (ε = 13500 M^{-1} cm^{-1}) in the UV-vis spectrum whereas **2** shows a strong band at 320 nm (ε = 12000 M^{-1} cm^{-1}) and a broad absorbance at 420 nm (ε = 5000 M^{-1} cm^{-1}). The ^1H NMR spectrum (in CD_3CN) of complex **1** shows sharp, paramagnetically shifted peaks from +80 ppm to −15 ppm, consistent with a high-spin (hs) iron(II) (S = 2) center. In contrast, complex **2** shows broad paramagnetic peaks between +75 ppm to +12 ppm, indicative of a hs-iron(III) (S = 5/2) complex. An Evans method measurement of the magnetic moment of **2** in CD_3CN gives μ_{eff} = 5.97 μ_B at 298 K, consistent with an S = 5/2 spin ground state. The zero-field ^{57}Fe Mössbauer spectrum of **2** (80 K) is shown in Figure 3 together with that of **1** for comparison. Complex **1** exhibits a sharp quadrupole doublet with isomer shift (δ) and quadrupole splitting ($|\Delta E_Q|$) parameters typical of hs-iron(II), while complex **2** exhibits parameters that match for a hs-iron(III) ion. The vibrational data for **1** and **2** obtained by ATR-IR spectroscopy (Figure 4) exhibit strong bands at 2060 cm^{-1} and 2045 cm^{-1}, respectively, corresponding to the asymmetric stretch for the N_3 group, which shift to 1990 cm^{-1} and 1980 cm^{-1}, upon labeling with $^{15}N_3$. These shifts are consistent with a simple harmonic oscillator model, and confirm the assignments of these bands as arising from the azide ligands. The mechanism of formation of the cis-$Fe(OH)(N_3)(BNPA^{Ph2}O)$ complex has not been studied in detail, but it likely follows the proposed mechanism for the formation of $Fe^{III}(OH)(OTf)(BNPA^{Ph2}O)$, as well as the synthesis of other $Fe^{III}(OH)$ complexes from Fe^{II}/O_2.[40, 41] Our previously proposed mechanism for the formation of the $Fe^{III}(OH)(OTf)$ complex suggested that solvent was likely participating in the reaction with O_2, providing a potential hydrogen atom source for the final $Fe^{III}(OH)$ product.[28] The syntheses of **2** and **4** were routinely carried out in THF, which could be the hydrogen atom source for the production of the OH ligand, especially given the relatively low C-H BDFE of 92 kcal/mol

for THF.[42] Qualitative color changes also suggest that **2** and **4** can be formed in CH_3CN, but our previous work on $Fe^{III}(OH)(OTf)$ indicates that CH_3CN gives lower yields of this product, and therefore THF is used for all of the studies presented here. The high C-H BDFE for CH_3CN (96 kcal/mol)[42] suggests that this solvent may not be a good H-atom source. The low yields observed in CH_3CN may suggest that there is partial ligand degradation via intramolecular oxidation pathways, providing possible H-atom sources. Determining the detailed mechanism of formation of the $Fe^{III}(OH)$ complexes is challenging, and we are unable to provide a complete, balanced reaction for the formation of these complexes at this time. We do note that several other $Fe^{III}(OH)$ complexes are formed in a similar manner from iron(II) and excess O_2, but in these cases the mechanism and complete stoichiometry is also not available.[40, 41, 43] These questions provide motivation for further study regarding the mechanism of $Fe^{III}(OH)$ formation from Fe^{II}/O_2.

Previously we reported[30] the characterization of a lithium adduct of the $Fe^{II}(OH)$ complex $Fe^{II}(BNPA^{Ph2}O)(OH)$•(Li(OTf)(THF)) (**3**) (**3-Li$^+$**), which was isolated by crystallization from THF/pentane using LiOH as the OH^- source. The Li^+ ion was found to make a bridge between the alkoxo donor of the ligand ($BNPA^{Ph2}O$) and the terminal hydroxide (OH) group. However, we were previously unsuccessful in crystallizing **3** in the absence of Li^+ ions. Modification of the synthesis by replacing liOH with potassium tert-butoxide in wet THF has led to crystallization of **3** (Figure 1c) without the bound Li^+ ion. A comparison of the structures of **3** and **3-Li$^+$** (Figure S44) reveals a slight elongation of both the Fe–OH and Fe–alkoxide bonds due to Li+ coordination; d(Fe–OH) = 1.9584(9)Å and d(Fe–alkoxide) = 1.9318(9) Å in **3** whereas d(Fe–OH) = 1.9874(14) Å and d(Fe–alkoxide) = 1.9719(13) Å in **3-Li$^+$**. The average H-bonding distance between the OH and amine groups is shorter in **3** as compared to **3-Li$^+$**; d_{ave}(N(H)–O(H)) = 2.7876(11) Å in **3** whereas d_{ave}(N(H)–O(H)) = 2.8985 (14) Å in **3-Li$^+$**.

Complex **5**, $Fe^{II}(BNPA^{Ph2}O)(NCS)$ was synthesized by addition of 1 equiv of KSCN to the $Fe^{II}(BNPA^{Ph2}O)(Br)$ precursor, and characterized by single crystal X-ray diffraction (XRD) (Figure 2a). Upon addition of dry O_2 to complex **5**, an immediate change in color from yellow to bright orange was observed. Workup followed by crystallization using THF/pentane gave dark orange crystals suitable for XRD. Structural data reveals a six-coordinate complex, $Fe^{III}(BNPA^{Ph2}O)(OH)(NCS)$ (**4**), where a terminal OH ligand is positioned in the H-bonding site and the pseudohalogen NCS is in the equatorial position, trans to the pyridine ligand (Figure 2b). We also synthesized the bis(isothiocyante) analog of complex **4**, i.e., $Fe^{III}(BNPA^{Ph2}O)(NCS)_2$ (**6**). Complex **6** was synthesized by substitution of Cl^- for SCN^- with the starting complex $Fe^{III}(BNPA^{Ph2}O)(Cl)_2$.[27] The structure of **6** reveals the expected six-coordinate complex with NCS- occupying both axial and equatorial positions (Figure 2c).

Complex **5** shows a strong band at 325 nm (ε = 17000 M^{-1} cm^{-1}) in THF whereas complex **4** shows strong bands at 320 nm (ε = 19000 M^{-1} cm^{-1}) and 370 nm ((ε = 13400 M^{-1} cm^{-1}), and **6** show strong bands at 320 nm (ε = 13600 M^{-1} cm^{-1}) and 435 nm (ε = 19000 M^{-1} cm^{-1}). Similar to the iron(II) azide complex, ^{1}H NMR spectra of the iron(II) isothiocyanate complex shows sharp paramagnetic peaks in the range of +80 to −17 ppm, whereas the Fe(III) complexes (**4** and **6**) show much broader paramagnetic features. Complex **5** exhibits

a sharp peak in the ATR-IR spectrum at 2030 cm^{-1}, corresponding to the C=N stretch of the axial NCS ligand which shifts to 2055 cm^{-1} upon oxidation to complex **4**. This new band arises from the equatorial NCS ligand. Complex **6**, on the other hand, shows two strong peaks at 2015 and 2053 cm^{-1} corresponding to the two different NCS ligands.

Reactivity.

The reaction of $Fe^{III}(BNPA^{Ph2}O)(OH)(N_3)$ **(2)** with trityl radical (Ph_3C•) was studied to determine the relative selectivity between •OH versus •N_3 transfer to the carbon radical (Scheme 3). Addition of excess $(Ph_3C)_2$ (20 equiv) to a THF solution of **2** led to a color change from orange to yellow over the course of 4 h under light limiting conditions. The volatiles were removed, and the residue was dissolved in CD_3CN and subjected to NMR spectroscopy. The ^1H NMR spectrum of the reaction mixture shows formation of relatively sharp peaks which matches closely with **1**. There is also a broad peak that corresponds to a small amount of unreacted **2** (Figure 5).

The reaction between **2** and Ph_3C• was also monitored by ^{57}Fe Mössbauer spectroscopy (Figure 6). The reaction of isotopically enriched ^{57}Fe-**2** revealed a sharp quadrupole doublet as the major species (80% of the total iron fit) with $\delta = 1.00$ mm s^{-1}, $|\Delta E_Q| = 2.73$ mm s^{-1}, corresponding to the $Fe^{II}(N_3)$ complex **1**. A minor subcomponent (20% of total fit) with $\delta = 0.44$ mm s^{-1}, $|\Delta E_Q| = 1.10$ mm s^{-1}, corresponds to unreacted **2.** These data indicate selective OH• transfer over N_3• transfer. The alcohol product (Ph_3COH) was detected by ^1H NMR spectroscopy, leading to formation of a singlet at $\delta = 5.50$ ppm which can be assigned to the hydroxyl group. The NMR data gave a 75% yield of Ph_3COH. This result is analogous to our previous finding that showed hydroxylation was predominant over halogenation in an Fe(OH)(Cl) complex.[29] The dominance of hydroxylation over azidation is most likely due to the formation of the stronger C–OH bond over the weaker C–N_3 bond.[44]

Reaction of **2** with the substituted triphenylmethyl derivatives (p-^{t}Bu-$C_6H_4)_3C$• and (p-Cl-$C_6H_4)_3C$• lead only to hydroxylation (Figure S23), as seen for the unsubstituted (p-H-$C_6H_4)_3C$•. However, different results were obtained when the more electron-rich (p-OMe-$C_6H_4)_3C$• derivative was employed. Addition of 3 equiv of (p-OMe-$C_6H_4)_3C$• to **2** in THF leads to the disappearance of **2** by ^1H NMR spectroscopy, and formation of peaks corresponding to a mixture of the two iron(II) complexes **1** and **3**. The diamagnetic region of the ^1H NMR spectrum revealed the formation of the alcohol ((p-OMe-$C_6H_4)_3COH$) (30%), whereas the azide ((p-OMe-$C_6H_4)_3CN_3$) product was isolated by column chromatography in 40% yield and identified by NMR and ATR-IR spectroscopies. The IR data reveal a strong band at 2096 cm^{-1}, which matches for (p-OMe-$C_6H_4)_3CN_3$ (Figure 7). There is also a band observed at 2050 cm^{-1}, which corresponds to the starting material $Fe^{III}(BNPA^{Ph2}O)(OH)(N_3)$. The NMR data on the crude reaction mixture under anaerobic conditions show no starting material remaining in this reaction, and therefore the $Fe^{III}(OH)(N_3)$ complex is presumed to be generated by exposure of the $Fe^{II}(N_3)$ product to air under the aerobic conditions of the ATR-IR analysis. The organic azide band (at 2096 cm^{-1}) downshifts to 2030 cm^{-1} with the use of ^{15}N-labeled **2** (Figure S39), consistent with formation of (p-OMe-$C_6H_4)_3C^{15}N_3$. These data confirm that N_3• transfer occurs in the reaction of **2**

and the more electron-rich (p-OMe-$C_6H_4)_3C$•, in contrast to the unsubstituted Ph_3C•, which results in OH• transfer only.

Effect of solvent and temperature.

While the reaction of **2** with Ph_3C• gives selective formation of Ph_3COH, it does not occur with complete conversion, and there is ~20% of the starting iron(III) complex **2** remaining at the end of the reaction (Figure 6). However, screening reaction conditions revealed that replacing THF with the higher polarity solvent DMF, did give complete conversion (Figure S24). Solvent polarity has been proposed to lower the reaction barrier for analogous rebound-like reactions with Mn porphyrin.[45] No change in selectivity of OH versus N_3 transfer was observed.

Conversion of **2** to **1** in THF was also influenced by temperature; lowering the reaction to −35 °C led to lower conversion, whereas higher conversions were observed at 70 °C (Figure S24**).** Previously it was found that the selectivity of nonheme iron-mediated •OH versus •SR transfer was strongly influenced by the reaction temperature,[30] but in this case, changing the temperature of the reaction of **2** and Ph_3C• showed no change in product selectivity.

Influence of H^+, Lewis acids, CO_2.

Computational studies on the nonheme iron halogenases have suggested that halogenation may be favored over hydroxylation via deactivation of the OH group. In one study, it was postulated that transfer of H^+ from arginine could deactivate OH• transfer,[46] while in another study reaction of the byproduct CO_2 with FeOH could give a bicarbonate ion, abolishing OH• rebound reactivity.[47] With complex **2** in hand, we could examine directly the effects of H^+, Lewis acids, and CO_2 on OH• rebound reactivity. Addition of 1 equiv of the proton donor $LutH^+BAr^{F5}{}_4$ to **2** causes a rapid color change from orange to dark red, which then converts to a dark yellow solution upon addition of Ph_3C•. Analysis by ^1H NMR and IR spectroscopies show that the azide product, Ph_3CN_3, not the alcohol, is formed. Similar results are obtained if the strong Lewis acid $Sc(OTf)_3$ is used in place of the lutidinium reagent. The presence of either Bronsted or Lewis acid inhibits •OH transfer from **2** to the carbon radical, leading to selective azidation. However, addition of excess CO_2 does not have the same effect, and OH• transfer for **2** is observed in the presence or absence of CO_2.

Further study of the reaction of $Sc(OTf)_3$ with **2** led to the isolation of a new species. Reaction of **2** with $Sc(OTf)_3$ (1 equiv) in THF causes a rapid color change from bright orange to dark red. Slow vapor diffusion of pentane into a concentrated THF solution of the new species yielded dark red crystals suitable for single crystal XRD. The X-ray structure (Figure 8) revealed a new complex, $Fe^{III}(BNPA^{Ph2}O)(N_3)(OTf)$, where the OH ligand in **2** is replaced by a triflate ligand (Scheme 4). Comparison of **2** and $Fe^{III}(BNPA^{Ph2}O)(N_3)(OTf)$ shows that the azide ligand has moved to the H-bonded site in $Fe^{III}(BNPA^{Ph2}O)(N_3)(OTf)$, and the OTf^- ligand is now *trans* to the alkoxide group. This structure indicates that the addition of Sc^{3+}, and by analogy $LutH^+$, leads to binding of the exogenous Lewis acid to the OH ligand, ultimately resulting in ligand exchange and selective azide transfer from the iron center.

NCS analog.

The $Fe(OH)(N_3)(BNPA^{Ph2}O)$ complex reacts with the electron-rich $(p\text{-}OMe\text{-}C_6H_4)_3C•$ derivative to give both OH• and N_3• transfer products, in contrast to other Fe(OH)(X) ($BNPA^{Ph2}O$) (X = Cl, Br, OAr, SAr) complexes, which transfer only OH• at room temperature. We hypothesized that the mixed reactivity observed for the azide complex may be observable with other similar, triatomic pseudohalogen ligands, and to test this idea we synthesized the isothiocyanate analog, $Fe^{III}(BNPA^{Ph2}O)(OH)(NCS)$ (**4**). Reaction of **4** with excess $(p\text{-}OMe\text{-}C_6H_4)_3C•$ leads only to the formation of the OH• transfer products $Fe^{II}(BNPA^{Ph2}O)(NCS)$ (**5**) and $(p\text{-}OMe\text{-}C_6H_4)_3COH$ (Scheme 5). In comparison, reaction of **4** with the electron-deficient $(p\text{-}Cl\text{-}C_6H_4)_3C•$ leads only to trace amounts of **5**, with **4** remaining mostly unreacted as seen by ^1H NMR. This lack of reactivity is likely due to the electron-poor nature of the chloro-substituted radical.

Reaction of the bis(isothiocyanate) analog, $Fe^{III}(BNPA^{Ph2}O)(NCS)_2$ (**6**) with $Ph_3C•$ gives NCS• transfer, resulting in $Fe^{II}(BNPA^{Ph2}O)(NCS)$ (**5**) and Ph_3C-NCS (85%) products (Scheme 5). These results show that SCN• transfer is possible in the absence of a competing OH• transfer pathway, and is similar to what was observed for $Fe^{III}(OH)(X)$ versus $Fe^{III}(X)_2$ (X = halogen) complexes.[29] Taken together, our results on the NCS complexes show that OH• transfer is exclusively favored over NCS• transfer from iron(III) to the tertiary carbon radical derivatives, and is different from the $Fe^{III}(OH)(N_3)$ complex **2**.

Catalytic azidation.

To determine if **1** could serve in a catalytic role for the azidation of C-H bonds via azide rebound, we examined the reaction of Ph_3CH as test substrate with Zhdankin's λ^3-azidoiodane as oxidant and azide source. Similar conditions were used previously with iron(II) and tridentate, N_3 donor pybox ligands for the catalytic azidation of $C(sp^3)$-H bonds.[20–22] Reaction of Ph_3CH (1 equiv) with a slight excess of λ^3-azidoiodane (3 equiv) and **1** (10 mol%) as catalyst in CH_3CN at 50 °C led to the azidation of the $C(sp^3)$-H bond of the substrate. Workup and isolation of the azidation product by silica gel chromatography gave an isolated yield of 84% for Ph_3CN_3. Control reactions without **1** added as catalyst led to unreacted starting materials. No conversion was observed when the reaction was carried out at 23 °C, indicating that modest heating is required to carry out the catalysis reaction.

Addition of λ^3-azidoiodane to **1** in the absence of Ph_3CH leads to an immediate color change from yellow to dark red. Analysis of the reaction mixture by ATR-IR spectroscopy reveals two strong bands at 2074 cm^{-1} and 2046 cm^{-1}, which matches with $Fe^{III}(BNPA^{Ph2}O)(N_3)_2$ (**7**) (Figure 9). Complex **7** was independently synthesized by addition of 2 equiv of NaN_3 to the previously reported $Fe^{III}(BNPA^{Ph2}O)(Cl)_2$.[29] This complex reacts with $Ph_3C•$ to give Ph_3CN_3 (90%), indicating it is capable of efficient N_3• to carbon radicals. Although it is known certain Fe^{III} complexes can carry out C-H activation without an external oxidant,[48–53] we found that **7** shows only minor thermal decomposition in the presence of excess Ph_3CH at 50 °C, and there is no trace of the azidation product Ph_3CN_3.

A mechanism for catalytic azidation mediated by **1** is shown in Figure 9, based on our data and the proposed mechanism for the iron pybox catalysts.[20–22] The λ^3-azidoiodane

is activated by the Fe^{II} complex, releasing a carboxyl radical and generating the ferric intermediate **7,** followed by hydrogen atom abstraction by carboxyl radical. The $Ph_3C•$ can then undergo rebound with **7** as shown under non-catalytic conditions, giving the azidation product and the $Fe^{II}(N_3)$ starting complex **1**. It is possible that a mixed ligand complex $Fe^{III}(BNPA^{Ph2}O)(N_3)(OBz)$ (Bz = 2-I-C_6H_4CO) also forms in the catalytic reaction, which could undergo N_3 rebound as well.

Conclusions.

The synthesis, spectroscopic and structural characterization of a series of mononuclear, nonheme Fe^{II} and Fe^{III} complexes was carried out with the tetradentate, monoanionic, $BNPA^{Ph2}O^-$ ligand. This ligand provides neopentylamine hydrogen bonding groups in the secondary coordination sphere, proximate to an open site on the metal, allowing for the stabilization of a variety of monodentate anions. These anions include OH^-, N_3^-, and NCS^-, resulting in the isolation of rare *cis*-$Fe^{III}(OH)(X)$ complexes. The latter species mimic the proposed, key ferric intermediates in a variety of nonheme iron hydroxylases and halogenases.

The reactivity of the *cis*-$Fe^{III}(OH)(N_3)$ complex with the tertiary carbon radicals (*p*-X-$C_6H_4)_3C•$ (X = Cl, H, ^{t}Bu) gives only hydroxylated product. However, reaction with an electron-rich derivative with X = OMe leads to significant amounts of azidation product. Given that the electron-rich *p*-OMe-substituted radical should be more reactive in general toward radical rebound, we hypothesize that the change in rebound selectivity arises from a greater lowering of the kinetic barrier for $N_3•$ transfer than for the parallel barrier associated with OH• transfer. Previous calculations have shown that halogen transfer to $Ar^X{}_3C•$ radicals has a similar or lower kinetic barrier compared to OH• transfer, but in these cases the thermodynamic driving force for halogenation is unfavorable leading to reversible halogenation and only hydroxylated products.[54] However, in the case of the pseudohalogen N_3^-, transfer to (*p*-OMe-$C_6H_4)_3C•$ may be thermodynamically more favorable, providing a stronger driving force for rebound. In contrast, the rebound selectivity for the *cis*-$Fe^{III}(OH)(NCS)$ complex follows that of the halide complexes, showing only OH• rebound reactivity. The major structural difference between the azido and isothiocyanato complexes is that the distal atom of the triatomic donor (X^-) is N versus S, respectively. It is interesting to speculate that X• transfer requires C-X bond formation to occur through the distal, as opposed to proximal, atom of the triatomic ligands. The NCS• transfer would then initially form a relatively unstable C-S bond in the $Ar_3C(SCN)$ product, which could inhibit NCS• transfer to carbon radicals.

Addition of Lewis (Sc^{3+}) or Bronsted ($LutH^+$) acids to the azido complex **2** leads to complete loss of OH• rebound and preferential formation of the azidation product. However, addition of CO_2 has no effect on these reactions. These results are consistent with the computational predictions regarding the influence of H^+ on nonheme iron halogenases,[11, 46, 47, 55] but suggest that CO_2 generated from the α-KG cofactor is an unlikely factor in selecting for halogen transfer.

The observation of catalytic azidation activity for **1** with the test substrate Ph_3CH is in line with the expectations from the isolated rebound reactions described here. The

results presented lend good support to the proposed rebound mechanisms in nonheme iron enzymes and synthetic catalysts. They also show that there is selectivity preferences for radical rebound in *cis*-$Fe^{III}(OH)(X)$ species which do not rely on substrate orientation from an outer-sphere protein cavity, but rather arise from inherent thermodynamic and kinetic properties of the ferric intermediate and the carbon radical partner. Hence, these observations may be useful for the construction of nonnative enzymatic reactions, as well as new nonheme iron azidation/halogenation/hydroxylation catalysts.

EXPERIMENTAL SECTION.

General Considerations.

All syntheses and manipulations were conducted in an N_2-filled drybox (O_2 < 0.2 ppm, H_2O < 0.5 ppm) or using standard Schlenk techniques under an atmosphere of Ar unless otherwise noted. $Fe(OTf)_2$•2MeCN and $^{57}Fe(OTf)_2$•2MeCN were prepared according to a literature procedure.[56] Powdered ^{57}Fe metal (95.93%) was purchased from Cambridge Isotope Laboratories. Potassium hydride (30 wt% dispersion in mineral oil) was purchased from Sigma-Aldrich, washed several times with hexanes and dried under vacuum prior to use. Acetonitrile and acetonitrile-d_3 were distilled from CaH_2. Tetrahydrofuran, tetrahydrofuran-d_8, toluene and toluene-d_8 were dried over Na/benzophenone and subsequently distilled. Anhydrous 2-methyltetrahydrofuran and pentane (sure seal) were purchased from Sigma-Aldrich, and distilled over Na/benzophenone. All solvents were degassed by a minimum of three freeze–pump–thaw cycles and stored over freshly activated 3 Å molecular sieves in the drybox following distillation. All other non-deuterated solvents were obtained from a Pure-solv solvent purification system from Innovative Technologies, Inc. All other reagents were purchased from commercial vendors and used without further purification. The ligand $BNPA^{Ph2}OH$ was prepared by a literature procedure[28] and was dried over P_2O_5 for 12 h under vacuum before metalation. The complexes $Fe^{II}(BNPA^{Ph2}O)(Br)$,[29] $^{57}Fe^{II}(BNPA^{Ph2}O)(OTf)$,[28] $Fe^{III}(BNPA^{Ph2}O)(Cl)_2$[29] were synthesized following literature procedures. The $(Ph_3C)_2$ dimer,[31] triphenylmethylazide (Ph_3CN_3),[57] tris(p-methoxy-phenyl)methyl radical, tris(p-tert-butyl-phenyl)methyl radical, tris(p-chloro-phenyl)methyl radical,[26] PPN(N_3), and λ^3-azidoiodane,[23] were synthesized following literature procedures. Quantification of the triarylmethyl alcohol were done by a previously reported method.[26]

Instrumentation.

The ^1H and ^{19}F NMR spectra were measured on a Bruker 300 MHz or a Bruker 400 MHz NMR spectrometer. Chemical shifts were referenced to reported solvent resonances.[58] Midwest Microlab LLC (Indianapolis, IN) conducted elemental analyses on samples. UV–vis spectra were collected on a Cary 60 UV–vis spectrophotometer. Mössbauer spectra were recorded on a spectrometer from SEE Co. (Edina, MN) operating in the constant acceleration mode in a transmission geometry. A six-line iron metal Mössbauer spectrum was obtained using α-Fe foil (25 micron) at 298 K in a velocity scale of 10. The iron calibration procedure of WMOSS was used to fit the iron metal spectrum and obtain calibration constants. Samples were prepared in custom made Delrin cups and frozen in

liquid nitrogen prior to use. The samples were cooled in an SVT-400 cryostat from Janis Research Co. (Wilmington, MA), using liquid N_2 as a cryogen for 80 K measurements.

$Fe^{II}(BNPA^{Ph2}O)(N_3)$ (1).

The ligand $BNPA^{Ph2}OH$ (103 mg, 0.18 mmol) was dissolved in THF (2 mL) and a suspension of KH (7.3 mg, 0.18 mmol, 1 equiv) in THF (1 mL) was added. The solution was stirred for 1 h at 23 °C. An amount of anhydrous $FeBr_2$ (39.6 mg, 0.18 mmol, 1 equiv) was dissolved in acetonitrile (2 mL) and added dropwise to the $BNPA^{Ph2}OH$/KH mixture. An immediate color change from pale yellow to yellow-brown was noted, and the reaction mixture was stirred for 4 h. To this yellow-brown solution, an acetonitrile slurry of NaN_3 (11.8 mg, 0.182 mmol, 1 equiv) was added and the reaction mixture was stirred for an additional 12 h at 23 °C. A color change from yellow-brown to bright yellow was noted. The resulting dark yellow reaction mixture was evaporated to dryness under vacuum, giving a dark yellow solid. This solid was dissolved in a minimum amount of THF (3 mL) and passed through Celite to remove any insoluble impurities and the solution was left to stand with slow vapor diffusion of pentane. Dark yellow crystals (blocks, 120 mg (80%)) suitable for X-ray structure determination were obtained after 24 h. UV-vis (THF) λ_{max} (ε, M^{-1} cm^{-1}): 325 nm (12000). ^1H NMR (CD_3CN, 400 MHz): δ 74.08, 67.36, 59.61, 31.27, 22.20, 10.92, 9.25, 8.54, 7.36, 5.58, −0.34, −13.51 ppm. Elemental analysis: Anal. Calcd. $C_{36}H_{46}FeN_8O$•THF: C, 65.39; H, 7.41; 15.25. Found: C, 64.61; H, 7.35; N, 15.42. ATR-IR (ν_{azide}) = 2060 cm^{-1}. The ^{15}N-azide analog of complex **1** was synthesized following the same procedure using $Na^{15}N_3$. This complex shows an azide stretch at 1990 cm^{-1}. ^{57}Fe Mössbauer (solid film, 80 K): δ = 1.01 mm s^{-1}; $|\Delta E_Q|$ = 2.78 mm s^{-1}; $\Gamma_L = \Gamma_R$ = 0.28.

$Fe^{III}(BNPA^{Ph2}O)(OH)(N_3)$ (2).

Crystalline **1** (120 mg, 0.18 mmol) was dissolved in THF (5 – 10 mL). This solution was bubbled with excess, dry O_2 for 15 min, causing a rapid color change from yellow to dark red, which turned to bright orange over the course of 15 min. The solution was stirred for 30 min at 23 °C. The final orange solution was evaporated to dryness under vacuum to give a dark orange solid. This solid was washed with pentane to give a dark orange powder, which was then dissolved in THF and left to stand with slow vapor diffusion of pentane at 23 °C. Dark orange crystals (blocks, 90 mg (60%)) suitable for X-ray structure determination were obtained after 3 d. UV-vis (THF) λ_{max} (ε, M^{-1} cm^{-1}): 320 nm (13500), 420 nm (5000). ^1H NMR (CD_3CN, 400 MHz): δ 72.38, 16.09, 8.06, 7.31, 4.22, 3.42, −5.38. ppm. ATR-IR (ν_{azide}) = 2045 cm^{-1}. The ^{15}N-azide analog of complex **2** was synthesized following the same procedure using $Na^{15}N_3$. This complex shows an azide stretch at 1980 cm^{-1}. ^{57}Fe Mössbauer (solid film, 80 K): δ = 0.44 mm s^{-1}; $|\Delta E_Q|$ = 1.12 mm s^{-1}; $\Gamma_L = \Gamma_R$ = 0.44.

$Fe^{II}(BNPA^{Ph2}O)(OH)$ (3).

The ligand $BNPA^{Ph2}OH$ (146.0 mg, 0.26 mmol) was dissolved in THF (2 mL) and a suspension of KH (10.3 mg, 0.26 mmol, 1 equiv) in THF (1 mL) was added. The solution was stirred for 1 h at 23 °C. An amount of anhydrous $FeBr_2$ (55.4 mg, 0.26 mmol, 1 equiv) was dissolved in acetonitrile (2 mL) and added dropwise to the $BNPA^{Ph2}OH$/KH mixture. An immediate color change from pale yellow to yellow-brown was noted, and

the reaction mixture was stirred for 4 h. To this yellow-brown solution, a THF solution of KO^{t}Bu (29.0 mg, 0.26 mmol, 1 equiv) was added and the reaction mixture was stirred for an additional 12 h at 23 °C. A color change from yellow-brown to bright orange was noted. The resulting dark orange reaction mixture was evaporated to dryness under vacuum, giving a dark orange solid. This solid was dissolved in a minimum amount of THF (3 mL) and passed through Celite to remove any insoluble impurities. The solution was left to stand with slow vapor diffusion of pentane. Dark red crystals (blocks, 73 mg (45%)) suitable for X-ray structure determination were obtained after 24 h. ^{1}H NMR (CD_3CN, 400 MHz): δ 83.00, 74.91, 62.47, 56.71, 22.67, 17.13, 11.49, 11.00, 9.00 ppm. Elemental analysis: Anal. Calcd. $C_{36}H_{47}FeN_5O_2$: C, 67.81; H, 7.43; 10.98. Found: C, 67.71; H, 7.55; N, 10.41.

$Fe^{III}(BNPA^{Ph2}O)(OH)(NCS)$ (4).

Crystalline **5** (120 mg, 0.18 mmol) was dissolved in THF (5 – 10 mL). This solution was bubbled with excess, dry O_2 for 15 min, causing a rapid color change from yellow to bright orange. The solution was stirred for 30 min at 23 °C. The final orange solution was evaporated to dryness under vacuum to give a dark orange solid. This solid was washed with pentane to give a dark orange powder, which was then dissolved in THF and left to stand with slow vapor diffusion of pentane at 23 °C. Bright orange crystals (blocks, 90 mg (60%)) suitable for X-ray structure determination were obtained after 3 d. UV-vis (THF) λ_{max} (ε, M^{-1} cm^{-1}): 320 nm (19000), 370 nm (13400). ^{1}H NMR (CD_3CN, 400 MHz): δ 59.68, 46.74, 17.41, 15.59, 9.78, .57, 7.25, 6.62 ppm. Elemental analysis: Anal. Calcd. $C_{37}H_{47}FeN_6O_2S$: C, 63.88; H, 6.81; N, 12.08. Found: C, 63.17; H, 7.01; N, 11.94. ATR-IR (ν_{NCS}) = 2055 cm^{-1}.

$Fe^{II}(BNPA^{Ph2}O)(NCS)$ (5).

The ligand $BNPA^{Ph2}OH$ (103.0 mg, 0.18 mmol) was dissolved in THF (2 mL) and a suspension of KH (7.3 mg, 0.18 mmol, 1 equiv) in THF (1 mL) was added. The solution was stirred for 1 h at 23 °C. An amount of anhydrous $FeBr_2$ (39.6 mg, 0.18 mmol, 1 equiv) was dissolved in acetonitrile (2 mL) and added dropwise to the $BNPA^{Ph2}OH$/KH mixture. An immediate color change from pale yellow to yellow brown was noted, and the reaction mixture was stirred for 4 h. To this yellow-brown solution, KSCN (1 equiv) was added, and the reaction mixture was stirred for an additional 4 h at 23 °C. A color change from yellow brown to bright yellow was noted. The resulting dark yellow reaction mixture was evaporated to dryness under vacuum, giving a dark yellow solid. This solid was dissolved in minimum amount of THF (3 mL) and passed through Celite to remove any insoluble impurities and the solution was left to stand with slow vapor diffusion of pentane. yellow-green crystals (blocks, 120 mg (80%)) suitable for X-ray structure determination were obtained after 24 h. UV-vis (THF) λ_{max} (ε, M^{-1} cm^{-1}): 325 nm (17000). ^{1}H NMR (CD_3CN, 400 MHz): δ 77.72, 73.39, 59.16, 32.41, 22.42, 11.26, 10.35, 8.90, −16.07 ppm. Elemental analysis: Anal. Calcd. $C_{37}H_{46}FeN_6OS{\bullet}H_2O$: C, 63.78; H, 6.94; 12.06. Found: C, 64.05; H, 6.76; N, 12.16. ATR-IR (ν_{NCS}) = 2030 cm^{-1}.

$Fe^{III}(BNPA^{Ph2}O)(NCS)_2$ (6).

The ligand $BNPA^{Ph2}OH$ (69 mg, 0.12 mmol) was dissolved in THF (2 mL) and a suspension of KH (5 mg, 0.12 mmol, 1 equiv) in THF (1 mL) was added. The solution was stirred for 1 h at 23 °C. An amount of anhydrous $FeCl_3$ (20 mg, 0.12 mmol, 1 equiv) was dissolved in acetonitrile (2 mL) and added dropwise to the $BNPA^{Ph2}OH$/KH mixture. An immediate color change from colorless to dark red was noted, and the reaction mixture was stirred for 4 h. To this red solution, solid KSCN (24 mg, 0.24 mmol, 2 equiv) was added and the reaction mixture was stirred for an additional 12 h at 23 °C. The resulting red reaction mixture was evaporated to dryness under vacuum, giving a dark red solid. This solid was dissolved in a minimum amount of THF (3 mL) and passed through Celite to remove any insoluble impurities and the solution was left to stand with slow vapor diffusion of pentane. Dark red crystals (blocks, 60 mg (67%)) suitable for X-ray structure determination were obtained after 12 h. UV-vis (THF) λ_{max} (ε, M^{-1} cm^{-1}) = 320 nm (13600), 435 nm (10000). ^1H NMR (CD_3CN, 400 MHz): δ 73.13, 17.85, 14.10, 9.88, 8.50, 7.23, 5.36, −1.55 ppm. ATR-IR (ν_{NCS}) = 2053 and 2015 cm^{-1}.

$Fe^{III}(BNPA^{Ph2}O)(N_3)_2$ (7).

The ligand $BNPA^{Ph2}OH$ (74 mg, 0.13 mmol) was dissolved in THF (2 mL) and a suspension of KH (5.24 mg, 0.13 mmol, 1 equiv) in THF (1 mL) was added. The solution was stirred for 1 h at 23 °C. An amount of anhydrous $FeCl_3$ (21.0 mg, 0.13 mmol, 1 equiv) was dissolved in acetonitrile (2 mL) and added dropwise to the $BNPA^{Ph2}OH$/KH mixture. An immediate color change from colorless to dark red was noted, and the reaction mixture was stirred for 4 h. To this red solution, an acetonitrile slurry of NaN_3 (17.0 mg, 0.26 mmol, 2 equiv) was added and the reaction mixture was stirred for an additional 12 h at 23 °C. The resulting red reaction mixture was evaporated to dryness under vacuum, giving a dark red solid. This solid was dissolved in minimum amount of THF (3 mL) and passed through Celite to remove any insoluble impurities and the solution was left to stand with slow vapor diffusion of pentane. Dark red crystals (blocks, 70 mg (76%)) suitable for X-ray structure determination were obtained after 12 h. UV-vis (THF) λ_{max} (ε, M^{-1} cm^{-1}): 320 (10000), 425 (5100). ^1H NMR (CD_3CN, 400 MHz): δ 71.50, 16.07, 7.48, 5.22 ppm. ATR-IR (ν_{azide}) = 2070 and 2037 cm^{-1}. The ^{15}N-azide analog of complex **7** was synthesized following the same procedure using $Na^{15}N_3$. This complex shows two distinct azide stretches at 2000 and 1970 cm^{-1}.

$Fe^{III}(BNPA^{Ph2}O)(N_3)(OTf)$.

Complex **2** (50 mg, 0.07 mmol) was dissolved in THF (5 mL) and a THF solution of $Sc(OTf)_3$ (36 mg, 0.07 mmol, 1 equiv) was added dropwise. A color change from orange to dark red was observed. The reaction mixture was stirred at 23 °C for 30 min and then filtered through Celite to remove any solid impurities. The dark red filtrate was dried under vacuum to give a dark red powder. The solid was then dissolved in THF and left to stand with slow vapor diffusion of pentane at 23 °C. Dark red crystals (blocks, 30 mg (40%)) suitable for X-ray structure determination were obtained after 3 d. ^1H NMR (CD_3CN, 400 MHz): δ 72.38, 16.09, 8.06, 7.31, 4.22, 3.42, −5.38. ppm. ATR-IR (ν_{azide}) = 2076 cm^{-1}.

Synthesis of (p-OMe-$C_6H_4)_3CN_3$.

To an acetonitrile solution of (p-OMe-$C_6H_4)_3CCl$ (56 mg, 0.15 mmol), solid NaN_3 (10.0 mg, 0.15 mmol, 1 equiv) was added and the solution was stirred for 12 h at 23 °C. The color of the solution changes from dark orange to a turbid, pale yellow. The pale yellow solution was filtered through celite to remove insoluble impurities resulting in a clear yellow filtrate. The filtrate was dried down, washed with pentane and dried again to give a yellow solid as product. ^{1}H NMR (CD_2Cl_2), 400 MHz): δ 7.18–7.24 (m, 6H), 6.89–6.93 (m, 6H), 3.83 (s, 9H) ppm. ATR-IR (ν_{azide}) = 2100 cm^{-1}. The ^{15}N-azide analog of the compound was synthesized following the same procedure using $Na^{15}N_3$. This complex shows an azide stretch at 2030 cm^{-1}.

Preparation of Mössbauer samples for 1 and 2.

Crystalline $^{57}Fe^{II}$(BNPA^{Ph2}O)(OTf) (3 mg) was dissolved in CH_3CN (500 μL, 8 mM) and PPN(N_3) (1 equiv) was added, causing a color change from colorless to dark orange. The completion of the reaction to give ^{57}Fe-labeled **1** was verified by ^{1}H NMR spectroscopy. The solvent was removed, and the solid was dissolved in 2-MeTHF (300 μL, 11 mM) and transferred to a Mössbauer cup. The sample was then frozen in liquid nitrogen, and a Mössbauer spectrum of **1** was collected at 80 K in the absence of an external magnetic field. For the preparation of **2**, dry O_2 (2 mL) was added into a solution of ^{57}Fe-labeled **1** (500 μL) in a Mössbauer cup at 23 °C and a color change from yellow to orange was noted. The solution was left to stand for 15 min to ensure complete reaction. The solution was then dried under vacuum to create a thin film inside the cup. Mössbauer spectra were collected at 80 K. Mössbauer parameters (2-MeTHF, 80 K): $\delta = 1.02$ mm s^{-1}, $|\Delta E_Q| = 2.78$ mm s^{-1}, $\Gamma_L = \Gamma_R = 0.28$ for **1**, and $\delta = 0.44$ mm s^{-1}, $|\Delta E_Q| = 1.12$ mm s^{-1}, $\Gamma_L = \Gamma_R = 0.44$ for **2**.

Reaction of 2, 4, 6 and 7 with Ph_3C•.

In a typical reaction, an amount of crystalline complex (**2**, **4**, **6**, or **7**) was dissolved in THF (4 – 5 mg in 1 mL, 6 – 8 mM). To this solution, $(Ph_3C)_2$ (5 – 7 equiv, 10 – 14 equiv of Ph_3C•) was added and stirred in the dark at 23 °C. The reaction was stirred for 2–4 h until a color change from dark red or orange to yellow was observed. The reaction mixture was then dried down under vacuum and the resulting solid was dissolved in CD_3CN. ^{1}H NMR spectroscopy on this reaction mixture showed the formation of the respective, one-electron reduced Fe^{II} product, with no evidence for Fe^{III} complexes (see Supporting Information for spectra). ATR-IR spectroscopy on the final reaction mixture was used to identify the organic azide or isothiocyanate products.

Reaction of 2 with (p-X-$C_6H_4)_3C$•.

An amount of crystalline complex **2** was dissolved in 1 mL of THF. The para-substituted derivatives, (p-X-$C_6H_4)_3C$• (X = OMe, ^{t}Bu, Cl), were freshly prepared by using a literature procedure.[27] A toluene solution of the radical (200 mL, 2 equiv) was added to **2** in THF and stirred in the dark for 2 h. The solvents were removed under vacuum and the resulting solid was dissolved in CD_3CN for analysis by ^{1}H NMR spectroscopy. For analysis by ATR-IR spectroscopy, a small aliquot of the reaction mixture was placed directly on to the ATR-IR window and allowed to evaporate to dryness before the spectra were collected.

Reaction of 2 with Ph_3C• in the presence of H^+ or Sc^{3+}.

An amount of crystalline complex was dissolved in THF (4 – 5 mg in 1 mL, 6 – 8 mM). To this solution, 1 equiv of LutH($BArF^5_4$) (LutH = 2,6-lutidinium) or 1 equiv of $Sc(OTf)_3$ was added and a rapid color change from yellow-orange to dark red was noted. To this solution, $(Ph_3C)_2$ (5 – 7 equiv) was added and the reaction was stirred in the dark at 23 °C. An immediate color change to yellow was observed with the addition of $Sc(OTf)_3$, whereas the reaction with LutH($BArF^5_4$) gradually changed color from red to yellow over a period of 4 h. The reaction mixture was then dried down under vacuum and dissolved in CD_3CN. The diamagnetic region of the ^{1}H NMR spectrum did not show any peak at δ 4.46 ppm indicative of Ph_3COH. ATR-IR spectroscopy showed a peak at 2100 cm^{-1} for Ph_3CN_3.

Reaction of 2 with Ph_3C• in the presence of CO_2.

An amount of crystalline complex was dissolved in THF (4 – 5 mg in 1 mL, 6 – 8 mM) and stirred until fully dissolved. To this solution, dry CO_2 was bubbled for 20 min and no color change was noted. Excess $(Ph_3C)_2$ (5 – 7 equiv) was added and stirred in the dark at 23 °C for 4 h. The reaction mixture was then dried down and dissolved in CD_3CN. ^{1}H NMR spectroscopy showed formation of one-electron reduced complex **1**. In addition, ATR-IR spectroscopy did not show any formation of the organic azide product (Ph_3C-N_3).

Quantification of Ar_3COH in the reaction of 2 and Ar_3C•:

A stock solution was prepared by dissolving crystalline **2** (5 mg, 0.007 mmol) in THF-d_8 (1.5 mL, 4.96 mM). Solid $(Ph_3C)_2$ (11.4 mg, 0.0235 mmol, 10 equiv) was added to the stock solution of **2** in THF-d_8/toluene- d_8 (500 μL, 4.96 mM) and stirred in the dark for 4 h. An amount of trimethylphenylsilane (TMPS) (10 μL, 7 mM) was added as an internal standard, and the mixture was analyzed by ^{1}H NMR spectroscopy. A well-separated singlet at 5.50 ppm was observed, which was assigned to the OH proton of Ph_3COH based on comparison with an authentic sample. Integration of this peak and comparison with the TMPS standard gave a yield for Ph_3COH of 75%.

The same procedure as described for Ph_3COH was employed to quantify (p-OMe-$C_6H_4)_3COH$, except in this case, the starting radical was freshly prepared following a literature procedure.[25]

Quantification of (p-OMe-$C_6H_4)_3$C-N_3 in the reaction of 2 and (p-OMe-$C_6H_4)_3C$•.

An amount of **2** (70 mg, 0.10 mmol) was dissolved in THF (15 mL) and (p-OMe-$C_6H_4)_3C$• (5 equiv, stock solution in toluene) was added at 23 °C. The reaction was stirred for 4 h at 23 °C under light limiting conditions. The solvents were removed under vacuo and the dark red residue was dissolved in CH_2Cl_2 and the organic azide product (p-OMe-$C_6H_4)_3C$-N_3 was purified by silica gel column chromatography (9/1 v/v hexanes/EtOAc) to give an isolated yield of 12 mg (40%).

Quantification of Ph_3C-NCS in the reaction of 6 and Ph_3C•.

An amount of **6** (80 mg, 0.10 mmol) was dissolved in THF (15 mL) and $(Ph_3C)_2$ (10 – 20 equiv) was added at 23 °C. The reaction was stirred for 4 h at 23 °C under light limiting

conditions. The solvents were removed under vacuo and the dark red residue was dissolved in CH_2Cl_2 and the organic isothiocyanate product Ph_3C-NCS was purified by silica gel column chromatography (9/1 v/v hexanes/EtOAc) to give an isolated yield of 20 mg (85%).

Quantification of Ph_3C-N_3 in the reaction of 7 and Ph_3C•.

An amount of **7** (80 mg, 0.10 mmol) was dissolved in THF (15 mL) and $(Ph_3C)_2$ (10 – 20 equiv) was added at 23 °C. The reaction was stirred for 4 h at 23 °C under light limiting conditions. The solvents were removed under vacuo and the dark red residue was dissolved in CH_2Cl_2 and the organic azide product Ph_3C-N_3 was purified by silica gel column chromatography (9/1 v/v hexanes/EtOAc) to give an isolated yield of 25 mg (90%).

Catalytic azidation of Ph_3CH.

An amount of Ph_3CH (50 mg, 0.20 mmol) was dissolved in CH_3CN (1 mL). Crystalline complex **1** (13.3 mg, 0.02 mmol, 10 mol%) was added and the solution was stirred for 5 min at 50 °C. Solid λ^3-azidoiodinane (173 mg, 0.60 mmol, 3 equiv) was added and the reaction mixture was stirred for 16 h at 50 °C under light limiting conditions. The volatiles were removed under vacuum and the solid was redissolved in diethyl ether (5 mL) and stirred for 15 min. The ethereal solution was passed through a silica plug and the pale-yellow filtrate was dried down to give an oily solid mixture. The target compound (Ph_3C-N_3) was isolated using silica gel column chromatography (2% EtOAc/hexanes) to give an isolated yield of 47 mg (84%).

Supplementary Material

Refer to Web version on PubMed Central for supplementary material.

ACKNOWLEDGMENT

The NIH (GM119374 to D.P.G.) is gratefully acknowledged for financial support.

REFERENCES

1. Sahu S; Goldberg DP, Activation of Dioxygen by Iron and Manganese Complexes: A Heme and Nonheme Perspective. J. Am. Chem. Soc. 2016, 138, 11410–11428. [PubMed: 27576170]
2. Kovaleva EG; Lipscomb JD, Versatility of biological non-heme Fe(II) centers in oxygen activation reactions. Nat. Chem. Biol. 2008, 4, 186–193. [PubMed: 18277980]
3. Zaragoza JPT; Goldberg DP, Dioxygen Binding and Activation Mediated by Transition Metal Porphyrinoid Complexes. In Dioxygen-dependent Heme Enzymes, The Royal Society of Chemistry: 2019; 1–36.
4. Gordon JB; Goldberg DP, Sulfur-Ligated, Oxidative Nonheme Iron Enzymes and Related Complexes. In Comprehensive Coordination Chemistry III, Constable EC; Parkin G; Que L Jr, Eds. Elsevier: Oxford, 2021, 333–377.
5. Dunham NP; Arnold FH, Nature's Machinery, Repurposed: Expanding the Repertoire of Iron-Dependent Oxygenases. ACS Catal. 2020, 10, 12239–12255. [PubMed: 33282461]
6. Tanimoto H; Kakiuchi K, Recent applications and developments of organic azides in total synthesis of natural products. Nat. Prod. Commun. 2013, 8, 1021–34. [PubMed: 23980438]
7. Stanovnik B, Chapter Three - Application of organic azides in the synthesis of heterocyclic systems. In Advances in Heterocyclic Chemistry, Scriven EFV; Ramsden CA, Eds. Academic Press: 2020, 130, 145–194.

8. Chiba S, Application of Organic Azides for the Synthesis of Nitrogen-Containing Molecules. Synlett 2012, 2012, 21–44.
9. Hagenbuch J-P, Opportunities and Limits of the Use of Azides in Industrial Production. Implementation of Safety Measures. CHIMIA Intl. J. Chem. 2003, 57, 773–776.
10. Matthews ML; Chang W.-c.; Layne AP; Miles LA; Krebs C; Bollinger JM, Direct nitration and azidation of aliphatic carbons by an iron-dependent halogenase. Nat. Chem. Biol. 2014, 10, 209–215. [PubMed: 24463698]
11. Neugebauer ME; Sumida KH; Pelton JG; McMurry JL; Marchand JA; Chang MCY, A family of radical halogenases for the engineering of amino-acid-based products. Nat. Chem. Biol. 2019, 15, 1009–1016. [PubMed: 31548692]
12. Kim CY; Mitchell AJ; Glinkerman CM; Li F-S; Pluskal T; Weng J-K, The chloroalkaloid (−)-acutumine is biosynthesized via a Fe(II)- and 2-oxoglutarate-dependent halogenase in Menispermaceae plants. Nat. Commun. 2020, 11, 1867. [PubMed: 32313070]
13. Mitchell AJ; Dunham NP; Bergman JA; Wang B; Zhu Q; Chang W.-c.; Liu X; Boal AK, Structure-Guided Reprogramming of a Hydroxylase To Halogenate Its Small Molecule Substrate. Biochemistry 2017, 56, 441–444. [PubMed: 28029241]
14. Papadopoulou A; Meierhofer J; Meyer F; Hayashi T; Schneider S; Sager E; Buller R, Re-Programming and Optimization of a L-Proline cis-4-Hydroxylase for the cis-3-Halogenation of its Native Substrate. ChemCatChem 2021, 13, 3914–3919.
15. Chan NH, G. C., Vennelakanti V, Du Q, Kulik HJ, Lewis JC. Non-native Anionic Ligand Binding and Reactivity in Engineered Variants of the Fe(II)- and α-Ketoglutarate-Dependent Oxygenase, SadA. Inorg. Chem. 2022, 61, 14477–14485. [PubMed: 36044713]
16. Rui J; Zhao Q; Huls AJ; Soler J; Paris JC; Chen Z; Reshetnikov V; Yang Y; Guo Y; Garcia-Borràs M; Huang X, Directed evolution of nonheme iron enzymes to access abiological radical-relay Csp^3–H azidation. Science 2022, 376, 869–874. [PubMed: 35587977]
17. Timmins A; De Visser SP, A Comparative Review on the Catalytic Mechanism of Nonheme Iron Hydroxylases and Halogenases. Catalysts 2018, 8, 314.
18. Huang X; Bergsten TM; Groves JT, Manganese-Catalyzed Late-Stage Aliphatic C–H Azidation. J. Am. Chem. Soc. 2015, 137, 5300–5303. [PubMed: 25871027]
19. Huang X; Groves JT, Taming Azide Radicals for Catalytic C–H Azidation. ACS Catal. 2016, 6, 751–759.
20. Day CS; Fawcett A; Chatterjee R; Hartwig JF, Mechanistic Investigation of the Iron-Catalyzed Azidation of Alkyl C(sp3)–H Bonds with Zhdankin's λ^3-Azidoiodane. J. Am. Chem. Soc. 2021, 143, 16184–16196. [PubMed: 34559970]
21. Karimov RR; Sharma A; Hartwig JF, Late Stage Azidation of Complex Molecules. ACS Cent. Sci. 2016, 2, 715–724. [PubMed: 27800554]
22. Sharma A; Hartwig JF, Metal-catalysed azidation of tertiary C–H bonds suitable for late-stage functionalization. Nature 2015, 517, 600–604. [PubMed: 25631448]
23. Suh S-E; Chen S-J; Mandal M; Guzei IA; Cramer CJ; Stahl SS, Site-Selective Copper-Catalyzed Azidation of Benzylic C–H Bonds. J. Am. Chem. Soc. 2020, 142, 11388–11393. [PubMed: 32539355]
24. Pangia TM; Davies CG; Prendergast JR; Gordon JB; Siegler MA; Jameson GNL; Goldberg DP, Observation of Radical Rebound in a Mononuclear Nonheme Iron Model Complex. J. Am. Chem. Soc. 2018, 140, 4191–4194. [PubMed: 29537258]
25. Pangia TM; Yadav V; Gérard EF; Lin Y-T; de Visser SP; Jameson GNL; Goldberg DP, Mechanistic Investigation of Oxygen Rebound in a Mononuclear Nonheme Iron Complex. Inorg. Chem. 2019, 58, 9557–9561. [PubMed: 31313577]
26. Cummins DC; Alvarado JG; Zaragoza JPT; Effendy Mubarak MQ; Lin Y-T; de Visser SP; Goldberg DP, Hydroxyl Transfer to Carbon Radicals by Mn(OH) vs Fe(OH) Corrole Complexes. Inorg. Chem. 2020, 59, 16053–16064. [PubMed: 33047596]
27. Zaragoza JPT; Yosca TH; Siegler MA; Moënne-Loccoz P; Green MT; Goldberg DP, Direct Observation of Oxygen Rebound with an Iron-Hydroxide Complex. J. Am. Chem. Soc. 2017, 139, 13640–13643. [PubMed: 28930448]

28. Yadav V; Gordon JB; Siegler MA; Goldberg DP, Dioxygen-Derived Nonheme Mononuclear FeIII(OH) Complex and Its Reactivity with Carbon Radicals. J. Am. Chem. Soc. 2019, 141, 10148–10153. [PubMed: 31244183]
29. Yadav V; Rodriguez RJ; Siegler MA; Goldberg DP, Determining the Inherent Selectivity for Carbon Radical Hydroxylation versus Halogenation with FeIII(OH)(X) Complexes: Relevance to the Rebound Step in Non-heme Iron Halogenases. J. Am. Chem. Soc. 2020, 142, 7259–7264. [PubMed: 32281794]
30. Yadav V; Siegler MA; Goldberg DP, Temperature-Dependent Reactivity of a Non-heme FeIII(OH)(SR) Complex: Relevance to Isopenicillin N Synthase. J. Am. Chem. Soc. 2021, 143, 46–52. [PubMed: 33356198]
31. Jang ES; McMullin CL; Käß M; Meyer K; Cundari TR; Warren TH, Copper(II) Anilides in sp3 C-H Amination. J. Am. Chem. Soc. 2014, 136, 10930–10940. [PubMed: 24940616]
32. Lu X; Li X-X; Seo MS; Lee Y-M; Clémancey M; Maldivi P; Latour J-M; Sarangi R; Fukuzumi S; Nam W, A Mononuclear Nonheme Iron(IV)–Amido Complex Relevant for the Compound II Chemistry of Cytochrome P450. J. Am. Chem. Soc. 2019, 141, 80–83. [PubMed: 30558411]
33. Iovan DA; Betley TA, Characterization of Iron-Imido Species Relevant for N-Group Transfer Chemistry. J. Am. Chem. Soc. 2016, 138, 1983–1993. [PubMed: 26788747]
34. Bower JK; Cypcar AD; Henriquez B; Stieber SCE; Zhang S, C(sp^3)– H Fluorination with a Copper(II)/(III) Redox Couple. J. Am. Chem. Soc. 2020, 142, 8514–8521. [PubMed: 32275410]
35. Keshari K; Bera M; Velasco L; Munshi S; Gupta G; Moonshiram D; Paria S, Characterization and reactivity study of non-heme high-valent iron–hydroxo complexes. Chem. Sci. 2021, 12, 4418–4424. [PubMed: 34163706]
36. Li G; Estes DP; Norton JR; Ruccolo S; Sattler A; Sattler W, Dihydrogen Activation by Cobaloximes with Various Axial Ligands. Inorg. Chem. 2014, 53, 10743–10747. [PubMed: 25233022]
37. Vibbert HB; Neugebauer H; Norton JR; Hansen A; Bursch M; Grimme S, Hydrogen atom transfer rates from Tp-containing metal-hydrides to trityl radicals. Can. J. Chem. 2021, 99, 216–220.
38. Drummond MJ; Ford CL; Gray DL; Popescu CV; Fout AR, Radical Rebound Hydroxylation Versus H-Atom Transfer in Non-Heme Iron(III)-Hydroxo Complexes: Reactivity and Structural Differentiation. J.Am. Chem. Soc. 2019, 141, 6639–6650. [PubMed: 30969766]
39. Addison AW; Rao TN; Reedijk J; van Rijn J; Verschoor GC, Synthesis, structure, and spectroscopic properties of copper(II) compounds containing nitrogen–sulphur donor ligands; the crystal and molecular structure of aqua[1,7-bis(N-methylbenzimidazol-2′-yl)-2,6-dithiaheptane]copper(II) perchlorate. J. Chem. Soc, Dalton Trans. 1984, 1349–1356.
40. MacBeth CE; Golombek AP; Young VG; Yang C; Kuczera K; Hendrich MP; Borovik AS, O2 Activation by Nonheme Iron Complexes: A Monomeric Fe(III)-Oxo Complex Derived From O_2. Science 2000, 289, 938–941. [PubMed: 10937994]
41. Gordon Z; Miller TJ; Leahy CA; Matson EM; Burgess M; Drummond MJ; Popescu CV; Smith CM; Lord RL; Rodríguez-López J; Fout AR, Characterization of Terminal Iron(III)–Oxo and Iron(III)–Hydroxo Complexes Derived from O2 Activation. Inorg. Chem. 2019, 58, 15801–15811. [PubMed: 31714068]
42. Rayne S; Forest K, Gas phase homolytic bond dissociation enthalpies of common laboratory solvents: A G4 theoretical study. Nat. Prec. 2010.
43. Goldsmith CR; Stack TDP, Hydrogen Atom Abstraction by a Mononuclear Ferric Hydroxide Complex: Insights into the Reactivity of Lipoxygenase. Inorg. Chem 2006, 45, 6048–6055. [PubMed: 16842013]
44. Blanksby SJ; Ellison GB, Bond Dissociation Energies of Organic Molecules. Acc. Chem. Res. 2003, 36, 255–263. [PubMed: 12693923]
45. Liu W; Cheng M-J; Nielsen RJ; Goddard WA; Groves JT, Probing the C–O Bond-Formation Step in Metalloporphyrin-Catalyzed C–H Oxygenation Reactions. ACS Catal. 2017, 7, 4182–4188.
46. Huang J; Li C; Wang B; Sharon DA; Wu W; Shaik S, Selective Chlorination of Substrates by the Halogenase SyrB2 Is Controlled by the Protein According to a Combined Quantum Mechanics/Molecular Mechanics and Molecular Dynamics Study. ACS Catal. 2016, 6, 2694–2704.

47. de Visser SP; Latifi R, Carbon Dioxide: A Waste Product in the Catalytic Cycle of α-Ketoglutarate Dependent Halogenases Prevents the Formation of Hydroxylated By-Products. J. Phys. Chem. B. 2009, 113, 12–14. [PubMed: 19061416]
48. Gericke R; Doyle LM; Farquhar ER; McDonald AR, Oxo-Free Hydrocarbon Oxidation by an Iron(III)-Isoporphyrin Complex. Inorg. Chem. 2020, 59, 13952–13961. [PubMed: 32955871]
49. Lovisari M; Gericke R; Twamley B; McDonald AR, Comparing Metal–Halide and −Oxygen Adducts in Oxidative C/O–H Activation: Au^{III}–Cl versus Au^{III}–OH. Inorg. Chem. 2021, 60, 15610–15616. [PubMed: 34582177]
50. Mondal P; Lovisari M; Twamley B; McDonald AR, Fast Hydrocarbon Oxidation by a High-Valent Nickel–Fluoride Complex. Angew. Chem. Intl. Ed. 2020, 59, 13044–13050.
51. Mondal P; McDonald AR, Phenol Oxidation by a Nickel(III)–Fluoride Complex: Exploring the Influence of the Proton Accepting Ligand in PCET Oxidation. Chem. Eur. J. 2020, 26, 10083–10089. [PubMed: 32567726]
52. Mondal P; Pirovano P; Das A; Farquhar ER; McDonald AR, Hydrogen Atom Transfer by a High-Valent Nickel-Chloride Complex. J. Am. Chem. Soc. 2018, 140, 1834–1841. [PubMed: 29293330]
53. Panda C; Doyle LM; Gericke R; McDonald AR, Rapid Iron(III)−Fluoride-Mediated Hydrogen Atom Transfer. Angew. Chem. Intl. Ed. 2021, 60, 26281–26286.
54. Gérard EF; Yadav V; Goldberg DP; de Visser SP, What Drives Radical Halogenation versus Hydroxylation in Mononuclear Nonheme Iron Complexes? A Combined Experimental and Computational Study. J. Am. Chem. Soc. 2022, 144, 10752–10767. [PubMed: 35537044]
55. Mitchell AJ; Zhu Q; Maggiolo AO; Ananth NR; Hillwig ML; Liu X; Boal AK, Structural basis for halogenation by iron- and 2-oxo-glutarate-dependent enzyme WelO5. Nat. Chem. Biol. 2016, 12, 636–640. [PubMed: 27348090]
56. Albano S; Olivo G; Mandolini L; Massera C; Ugozzoli F; Di Stefano S, Formation of Imidazo[1,5-a]pyridine Derivatives Due to the Action of Fe^{2+} on Dynamic Libraries of Imines. J. Org. Chem. 2017, 82, 3820–3825. [PubMed: 28322557]
57. Bresien J; Schulz A; Thomas M; Villinger A, A Bismuth–Arene σ-Complex – On the Edge of Menshutkin-Type Complexes. Eur. J. Inorg. Chem. 2019, 2019, 1279–1287.
58. Fulmer GR; Miller AJM; Sherden NH; Gottlieb HE; Nudelman A; Stoltz BM; Bercaw JE; Goldberg KI, NMR Chemical Shifts of Trace Impurities: Common Laboratory Solvents, Organics, and Gases in Deuterated Solvents Relevant to the Organometallic Chemist. Organometallics. 2010, 29 (9), 2176–2179.

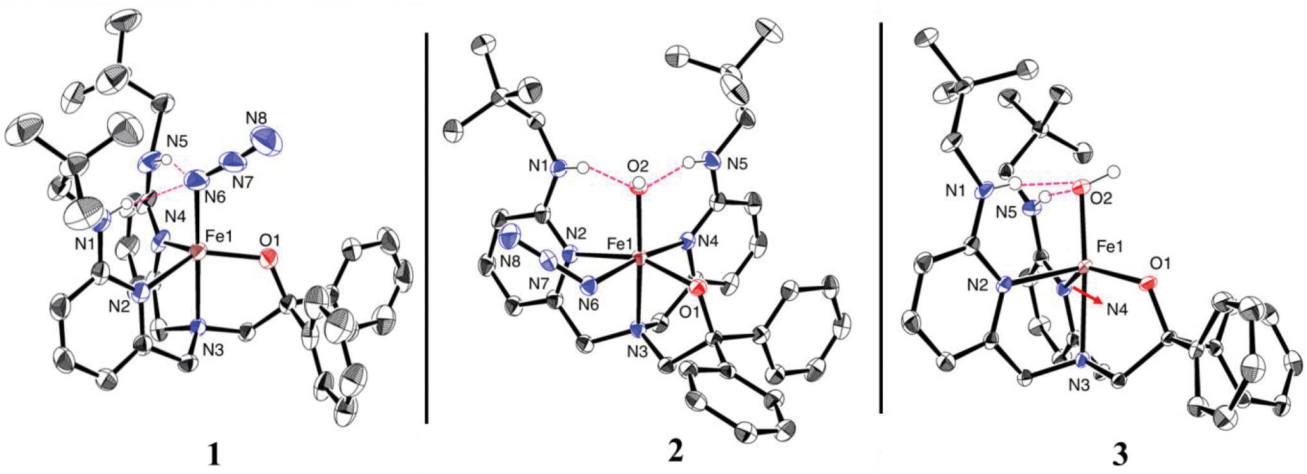

Figure 1.

Displacement ellipsoid plots (50% probability level) for **1** – **3** at 200(2) K for **1** and 110(2) K for **2** and **3**. Hydrogen atoms (except for N–H and O–H) omitted for clarity.

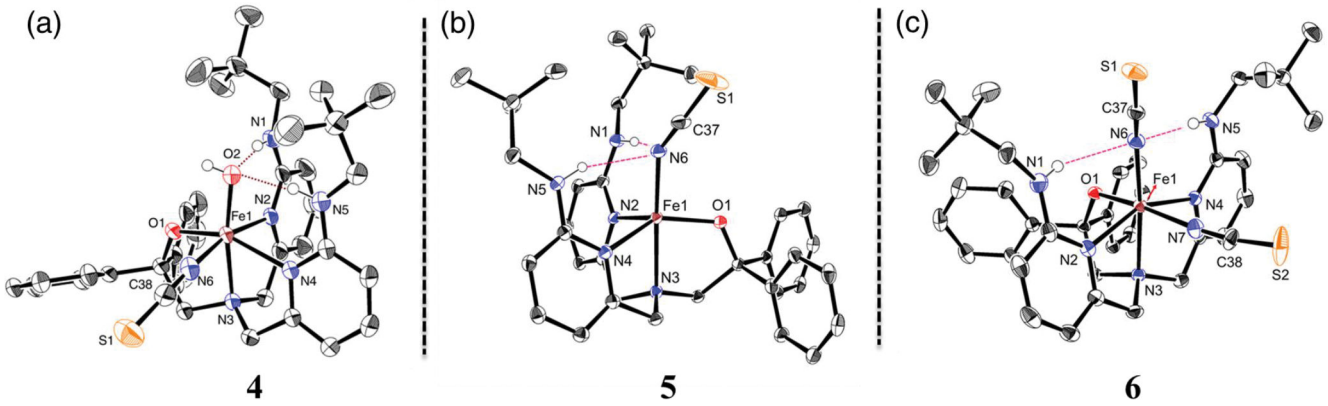

4 **5** **6**

Figure 2.

Displacement ellipsoid plots (50% probability level) for **4 – 6** at 110(2) K. Hydrogen atoms (except for N–H and O–H) omitted for clarity.

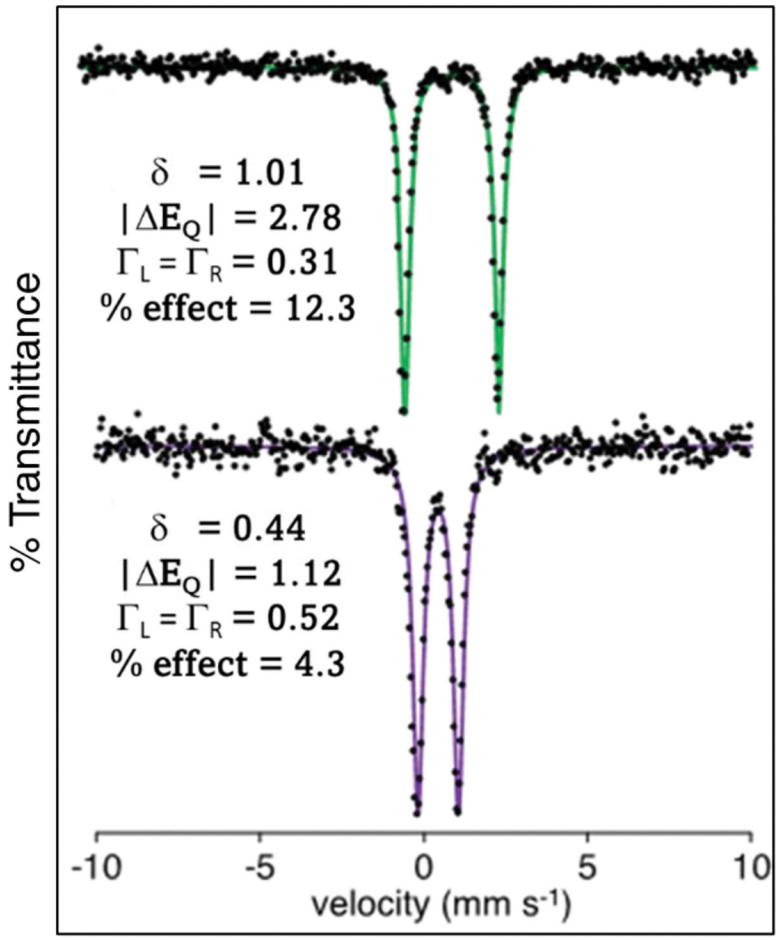

Figure 3.

Zero-field ^{57}Fe Mössbauer spectra (80 K) of $Fe^{II}(BNPA^{Ph2}O)(N_3)$ (**1**) in 2-MeTHF (top) and $Fe^{III}(BNPA^{Ph2}O)(OH)(N_3)$ (**2**) as a solid film (bottom). Experimental data (filled circles); best fits (solid lines). Fitting parameters (δ, $|\Delta E_Q|$, Γ) for each spectrum given in the figure.

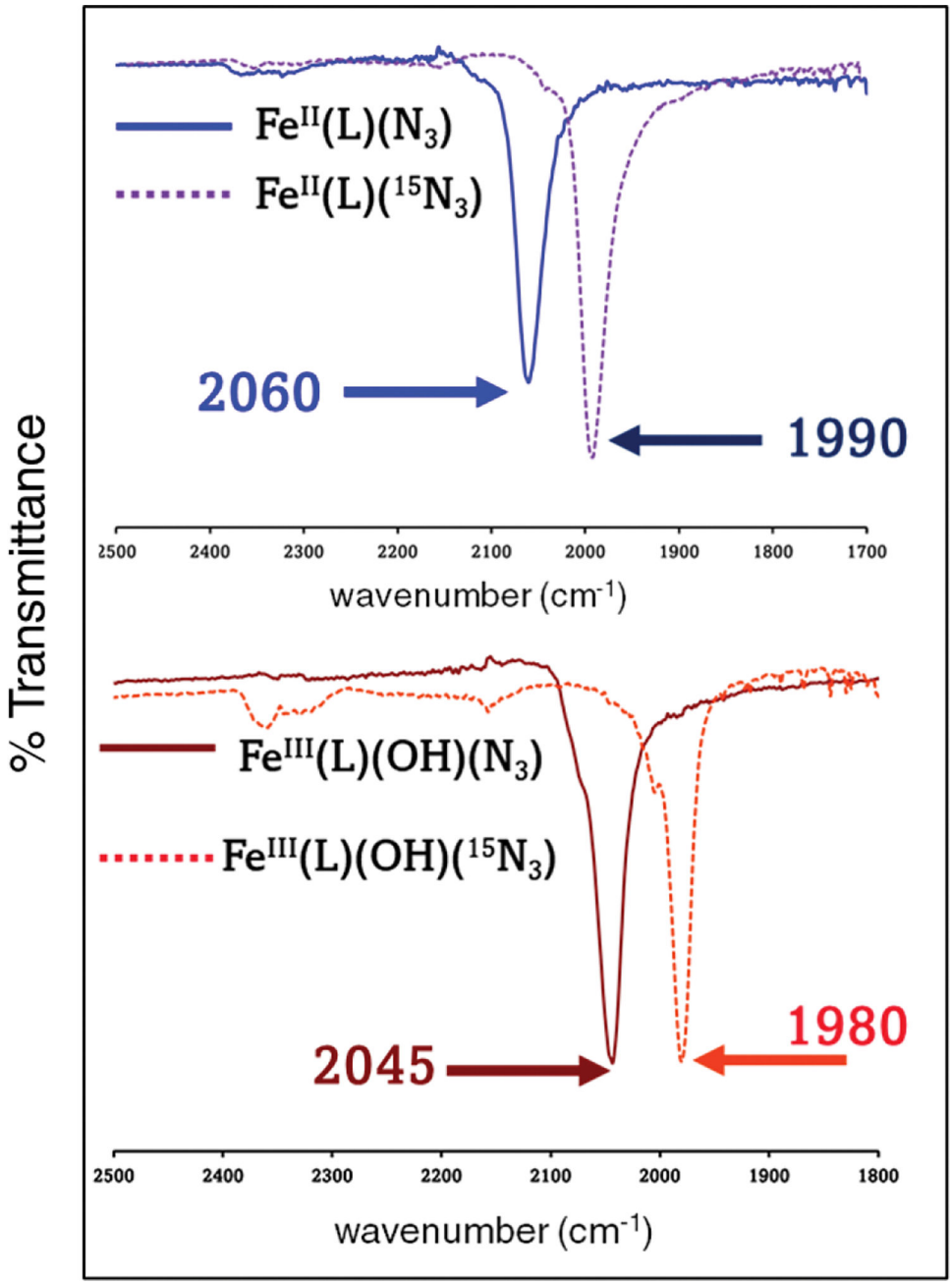

Figure 4.
Solid state ATR-IR spectra of **1**, **2** and their ^{15}N analogs (L = $BNPA^{Ph2}O$).

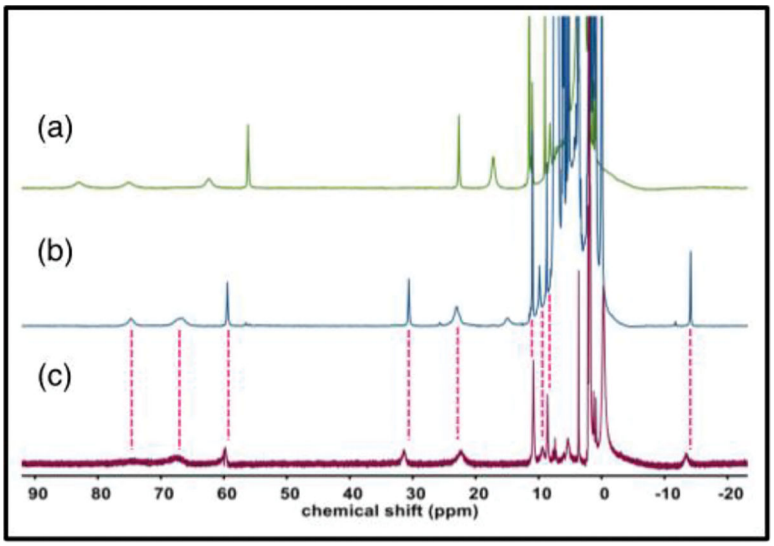

Figure 5.
^{1}H NMR spectra (CD_3CN, 298 K) of (a) **3**, (b) **2** + $Ph_3C^{\bullet}$ and (c) **1**.

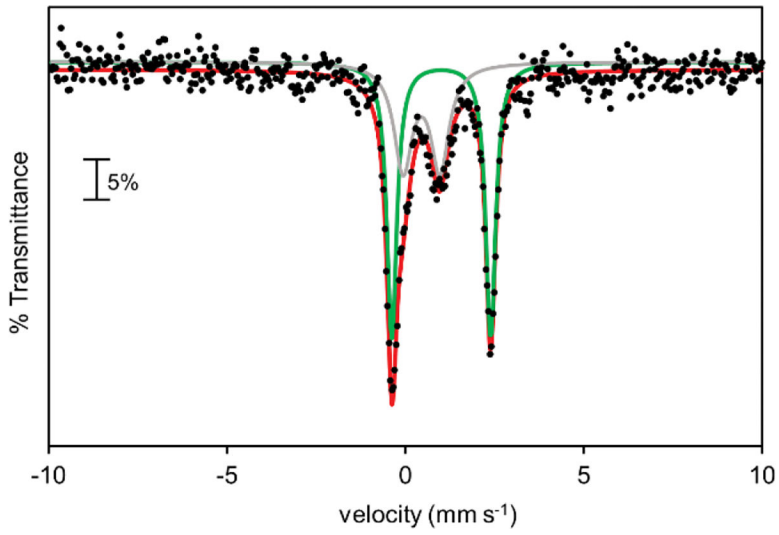

Figure 6.

Zero-field ^{57}Fe Mössbauer spectrum (80 K) (filled circles) of the reaction mixture of $Fe^{III}(BNPA^{Ph2}O)(OH)(N_3)$ (**2**) + Ph_3C• (10 equiv) in THF. Best fit (red line); major subcomponent: $\delta = 1.02$ mm s^{-1}, $|\Delta E_Q| = 2.77$ mm s^{-1} (green line, 80% of total fit); minor subcomponent: $\delta = 0.44$ mm s^{-1}, $|\Delta E_Q| = 1.10$ mm s^{-1} (grey line, 20% of total fit).

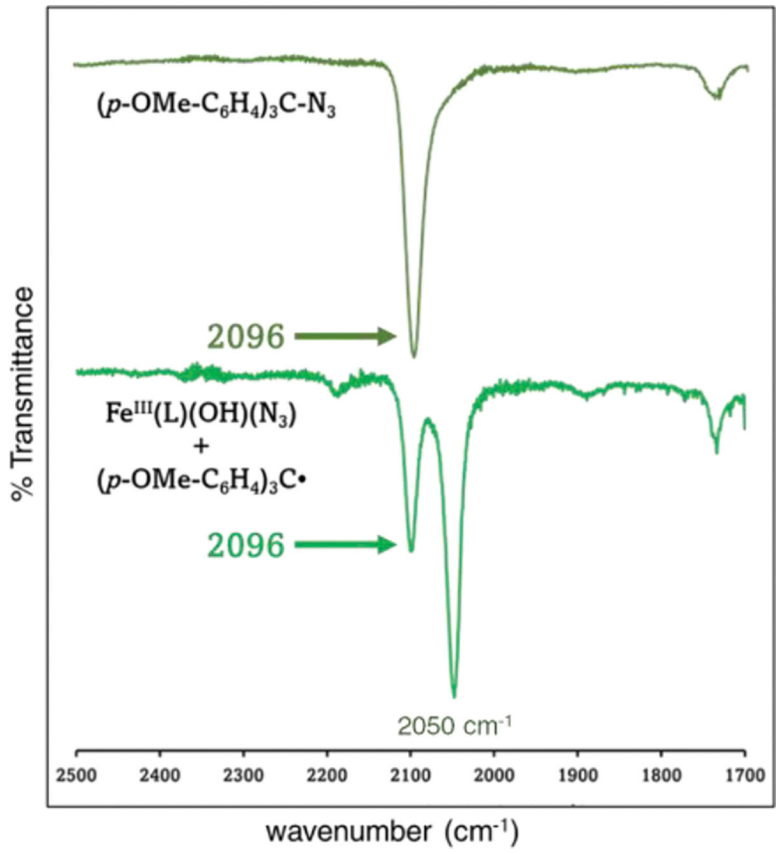

Figure 7.

ATR-IR spectra (solid film, 298 K) of the reaction mixture of **2** + (p-OMe-C_6H_4)$_3$C• (bottom), and (p-OMe-C_6H_4)$_3$CN_3 alone (top).

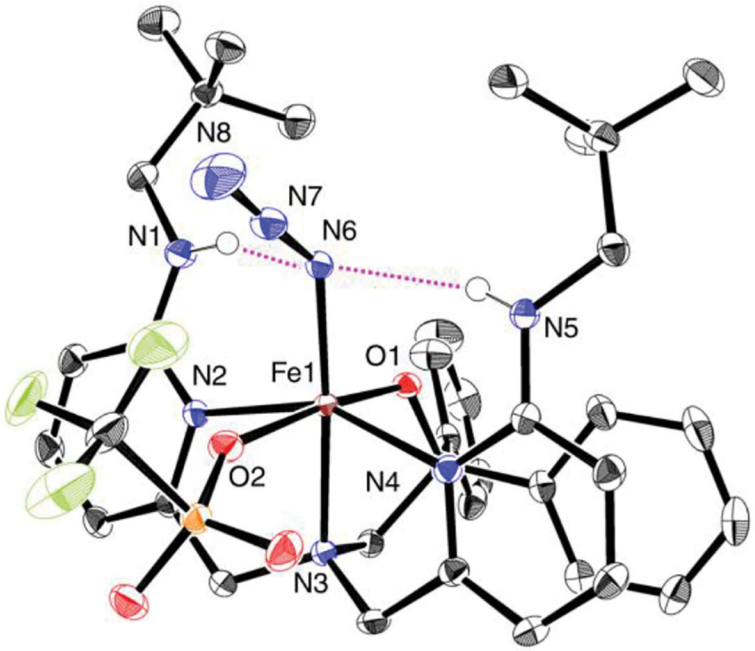

Figure 8.

Displacement ellipsoid plot (50% probability model) for $Fe^{III}(BNPA^{Ph2}O)(N_3)(OTf)$ at 110(2) K. Hydrogen atoms (except for N–H) omitted for clarity.

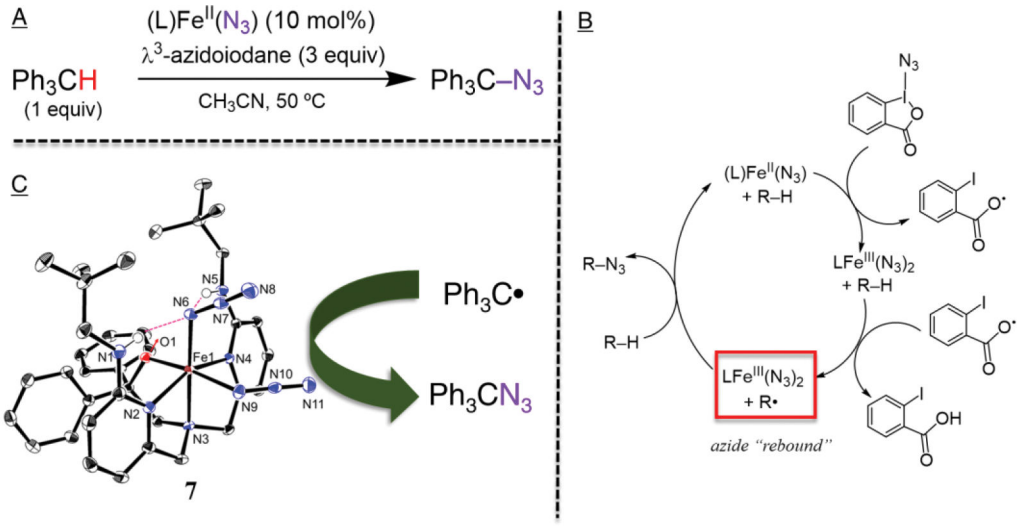

Figure 9.

(A) Catalytic azidation of triphenylmethane by **1**; (B) proposed mechanism;[22] and (C) displacement ellipsoid plot (50% probability level) for $Fe^{III}(BNPA^{Ph2}O)(N_3)_2$ (**7**) at 110(2) K with hydrogen atoms (except for N–H) omitted for clarity and its reactivity with $Ph_3C•$ (right).

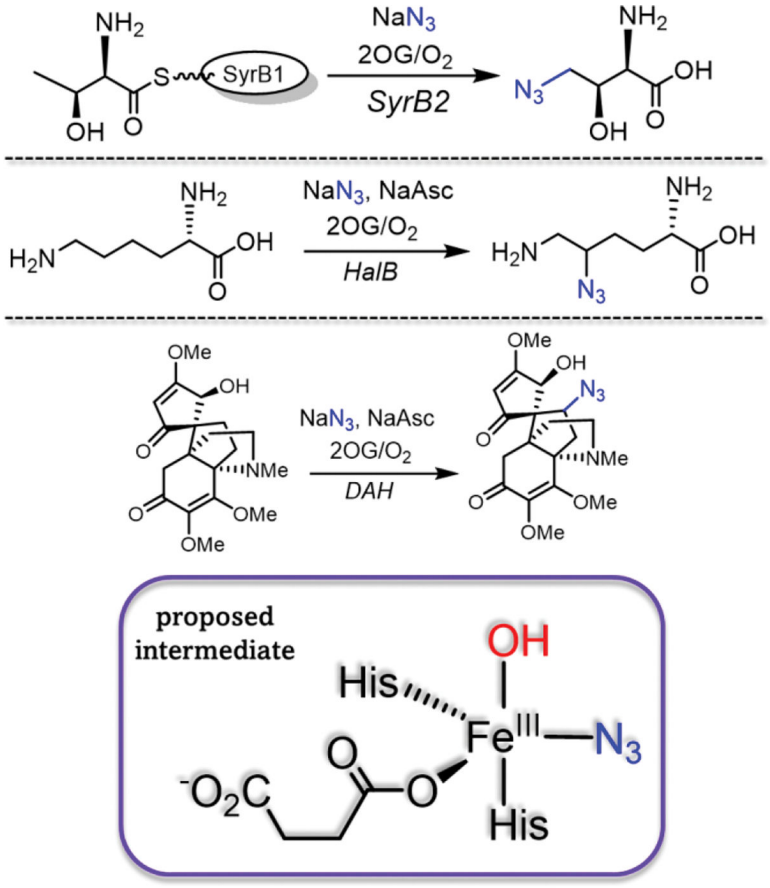

Scheme 1. Azidation by Nonheme Iron Enzymes.

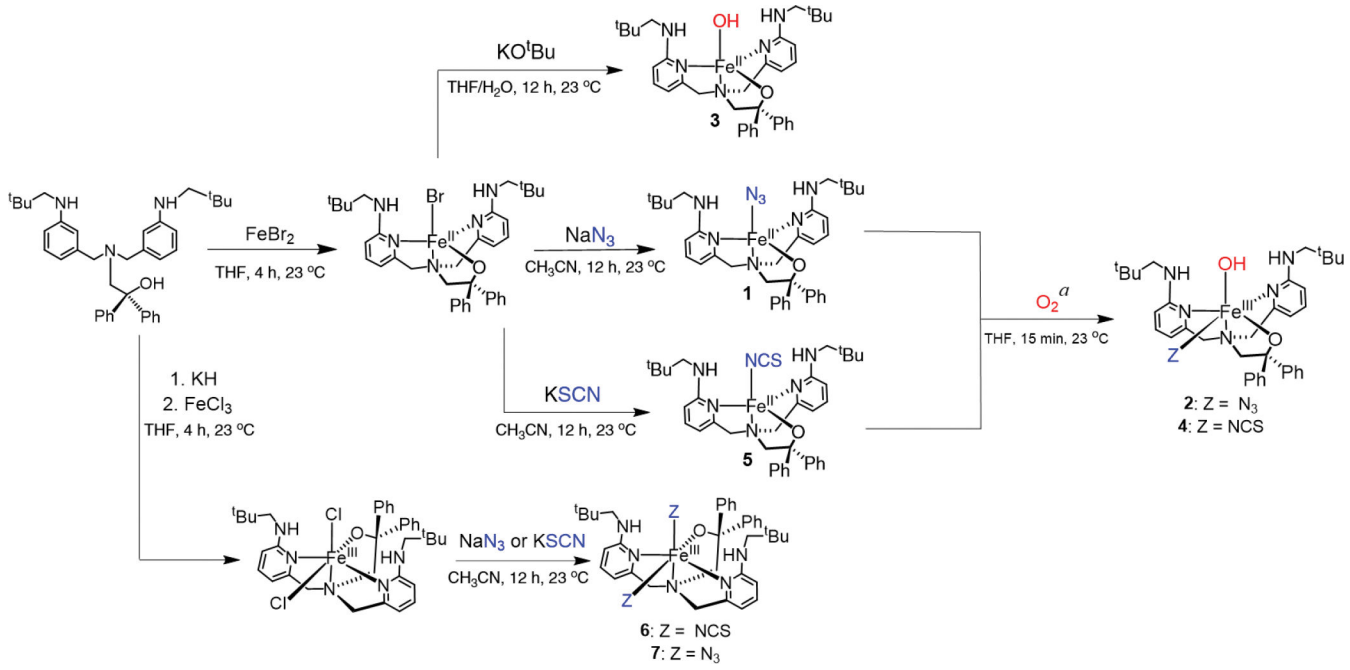

Scheme 2. Synthesis of Complexes 1 – 7

[a] A balanced chemical equation for the formation of **2** and **4**, from 1 and 5, respectively, is not provided due to the ambiguity of the H-atom source (see Discussion for details).

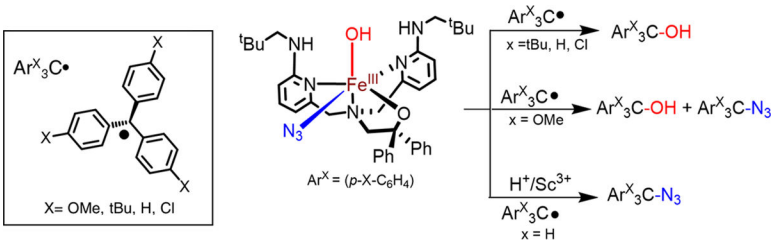

Scheme 3. Reaction of 2 with Triphenylmethyl Radical Derivatives.

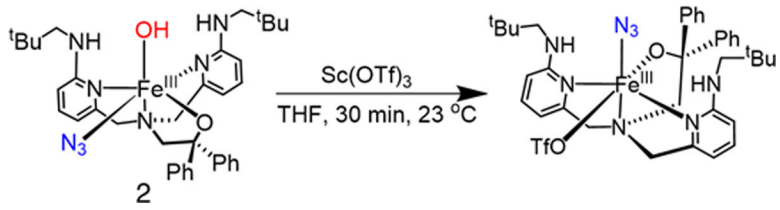

Scheme 4. Reaction of 2 with $Sc(OTf)_3$.

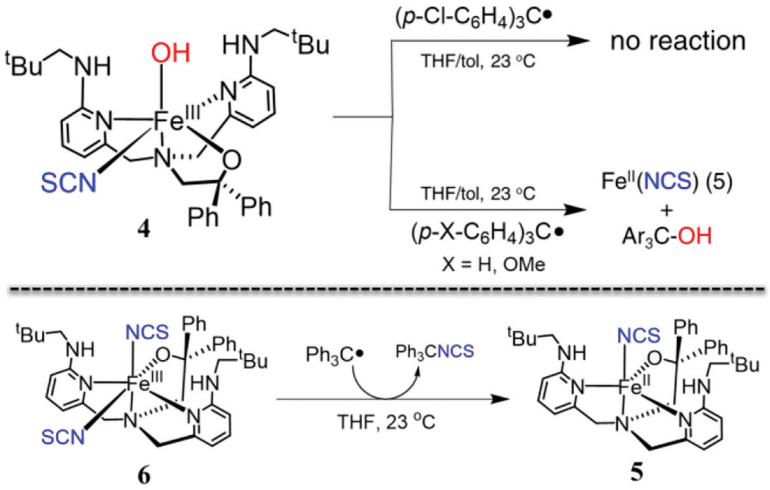

Scheme 5. Reactions of Complexes 4 and 6 with Ar_3C•